Supplementary Information

Nanocrystalline Fe-Fe_2O_3 Particle-Deposited N-doped Graphene as an Activity Modulated Pt-Free Electrocatalyst for Oxygen Reduction Reaction

Vishal M. Dhavale,[a,b] Santosh K. Singh,[a,b] Ayasha Nadeema,[a,b] Sachin S. Gaikwad,[a] Sreekumar Kurungot*,[a,b]

[a]*Physical and Materials Chemistry Division, National Chemical Laboratory, Pune-411008, India, Fax: +91-20-25902636; Tel: +91-20-25902566;*

E-mail: k.sreekumar@ncl.res.in

[b]*Academy of Scientific and Innovative Research (AcSIR), Anusandhan Bhawan, 2 Rafi Marg, New Delhi-110001, India.*

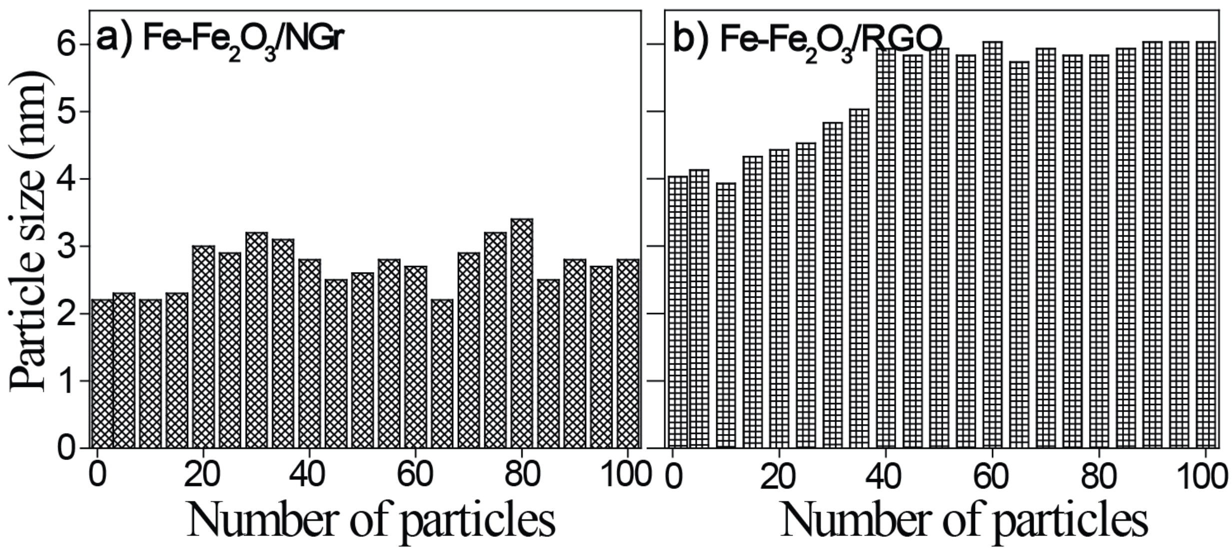

Figure S1: *Particle size histograms of Fe-Fe_2O_3/NGr (a), and Fe-Fe_2O_3/RGO (b).*

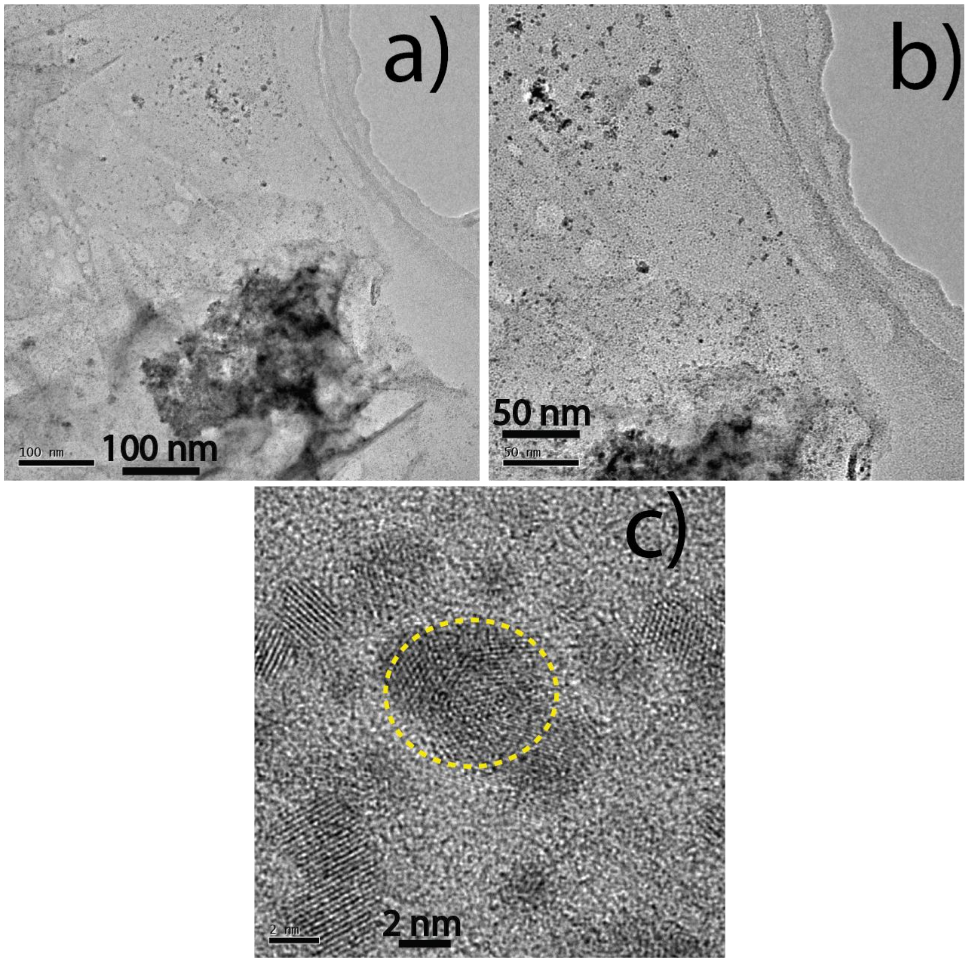

Figure S2: *TEM images of Fe-Fe_2O_3/RGO: a) and b) are the images taken at different magnifications and (c) HR-TEM image representing the lattice fringes. The boundary of a single Fe-Fe_2O_3 particle is marked with the yellow dotted circle.*

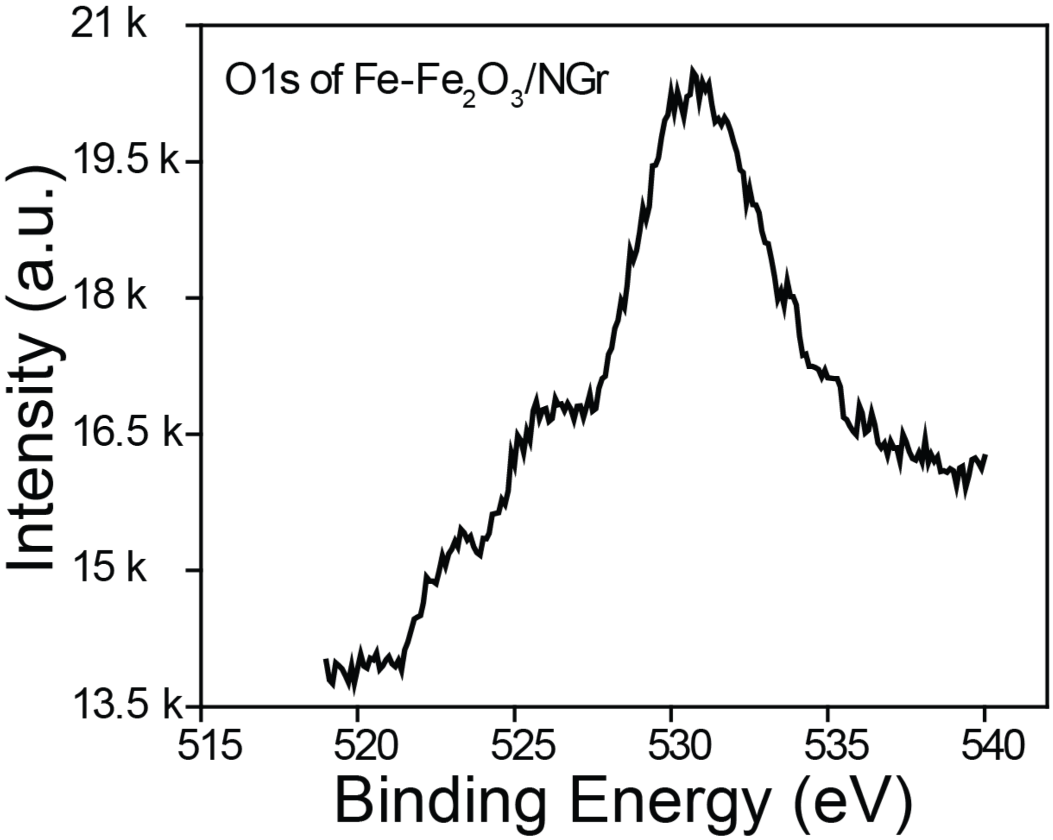

Figure S3: *XPS of O1s of Fe-*Fe_2O_3*/NGr.*

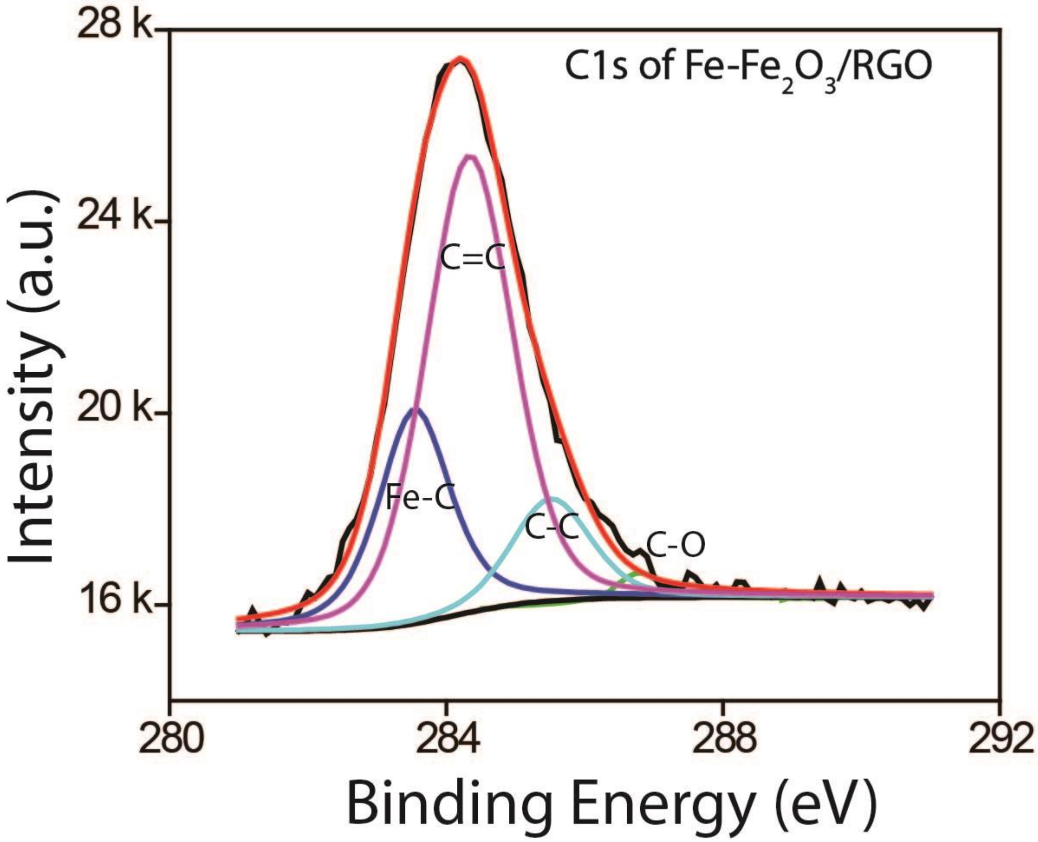

Figure S4: *Deconvulated XPS of C1s of Fe-Fe_2O_3/RGO. The peak at the lower binding energy (283.54 eV) indicates the interaction of Fe and C, whereas, the peaks at 284.33 and 285.51 eV are credited to the presence of sp^2(C=C) and sp^3 (C-C) carbons. Lastly, the peak at the higher binding energy of 286.35 eV indicates the presence of the oxygen functional groups on the carbon surface.*

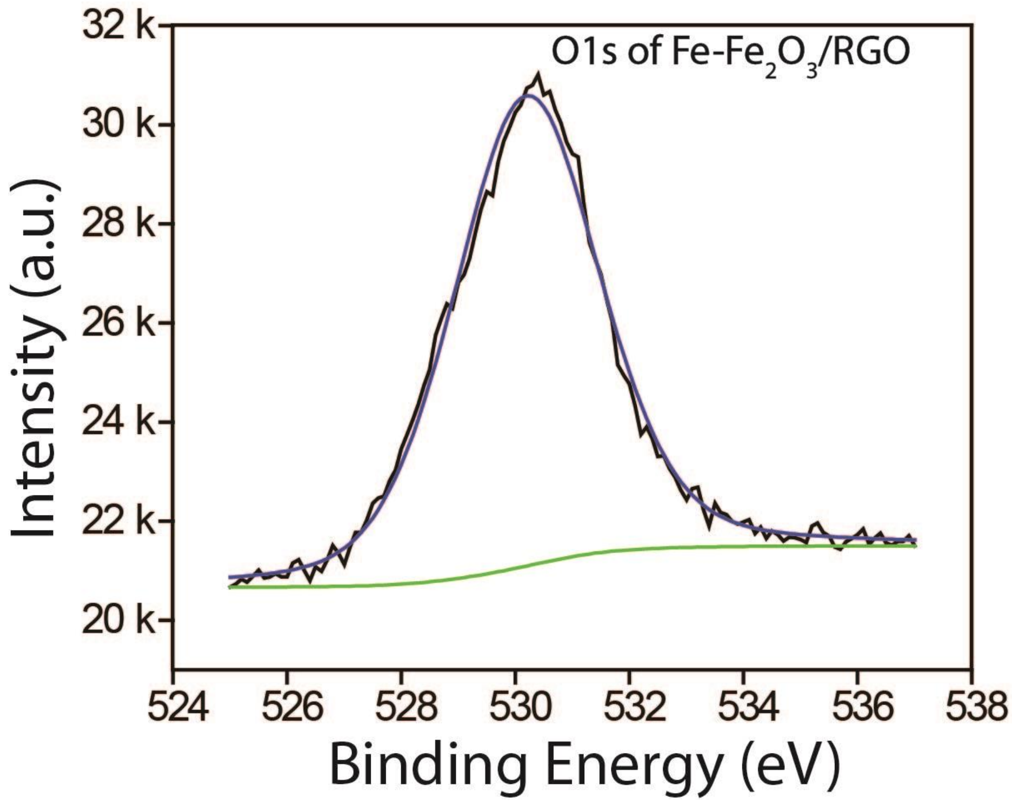

Figure S5: *XPS of O1s of Fe-Fe_2O_3/RGO.*

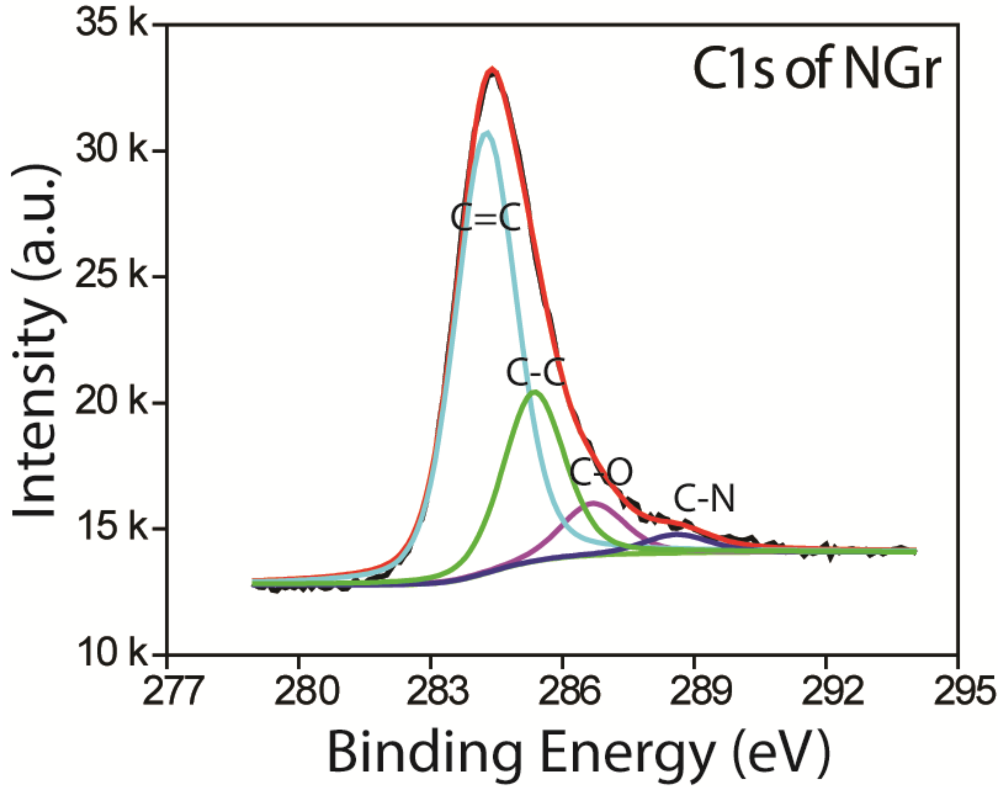

Figure S6: *Deconvulated XPS of C1s of NGr. The peaks at 284.34, 285.69, 286.72, and 287.80 eV are credited to the presence of C=C, C-C, C-O and C-N bonding, respectively. Peaks at the higher binding energy provide the evidence of 'C' coordination with the 'O' and 'N'.*

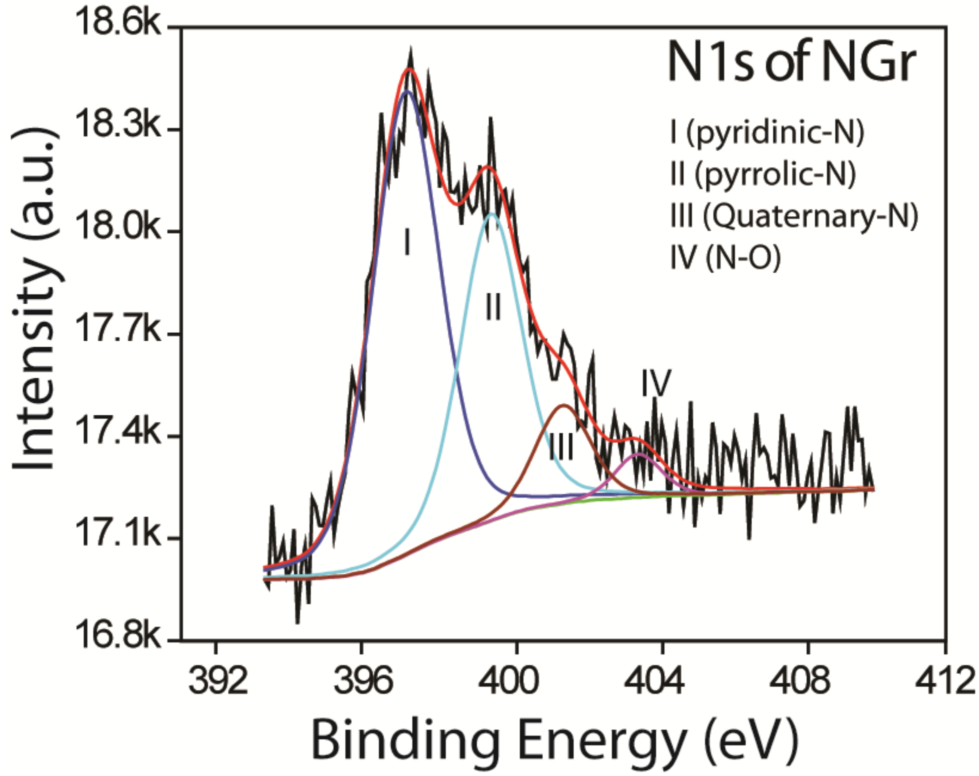

Figure S7: *Deconvulated XPS of N1s of NGr. The peaks at 398.34, 399.45, 401.98, and 403.62 eV are assigned to the presence of pyridinic-N, pyrrolic-N, quaternary-N and N-O bonding, respectively.*

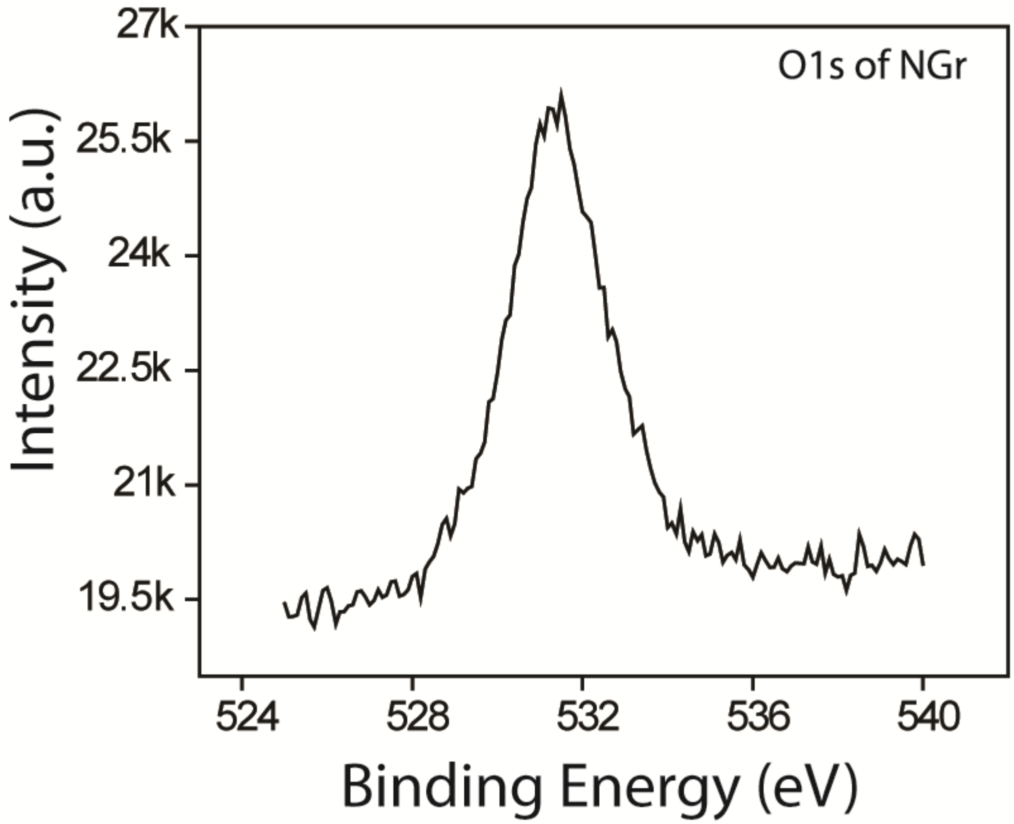

Figure S8: *Deconvulated XPS of O1s of NGr.*

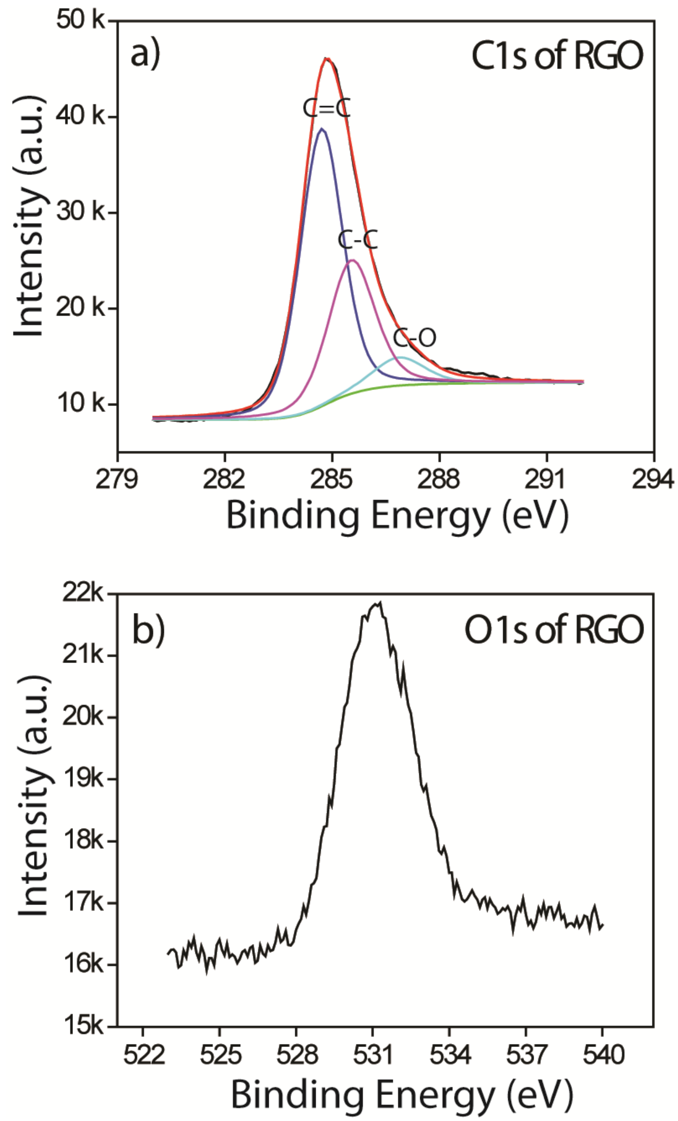

Figure S9: *(a) Deconvulated XPS of C1s of RGO. The peak at 284.70 and 285.50 eV are credited to the presence of the* sp^2 *(C=C) and* sp^3 *(C-C) carbons. Lastly, the peak at the higher binding energy (287.0 eV) indicates the presence of oxygen functional groups on the carbon surface; (b) XPS of O1s of RGO.*

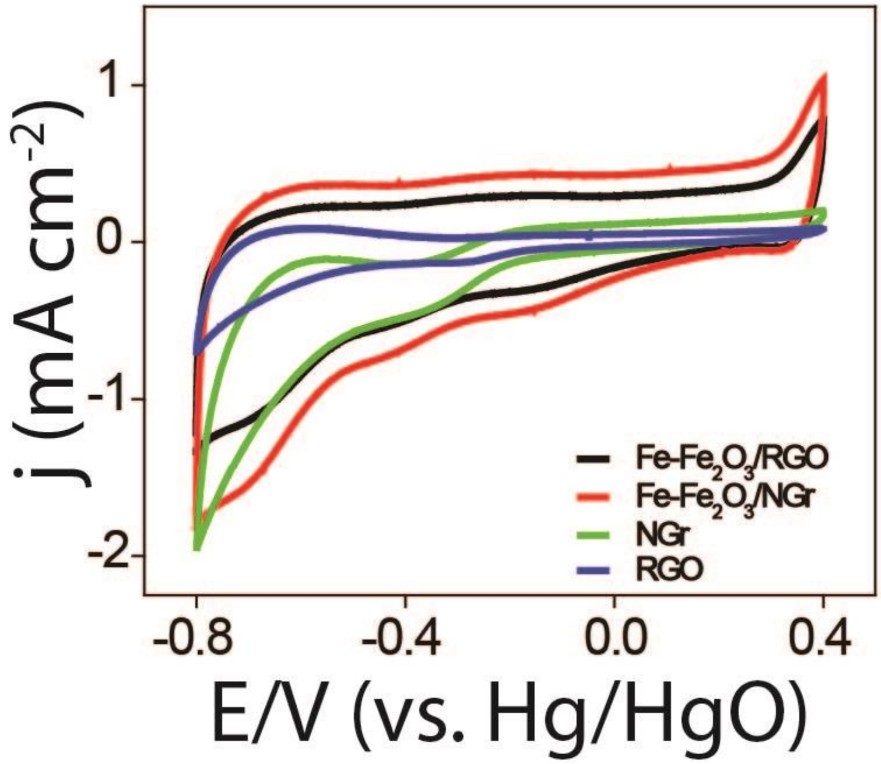

Figure S10: *Comparative cyclic voltammograms of Fe-Fe_2O_3/RGO, Fe-Fe_2O_3/NGr, NGr and RGO. Conditions: electrolyte: N_2- saturated 0.1 M KOH and scan rate: 20 mV/s.*

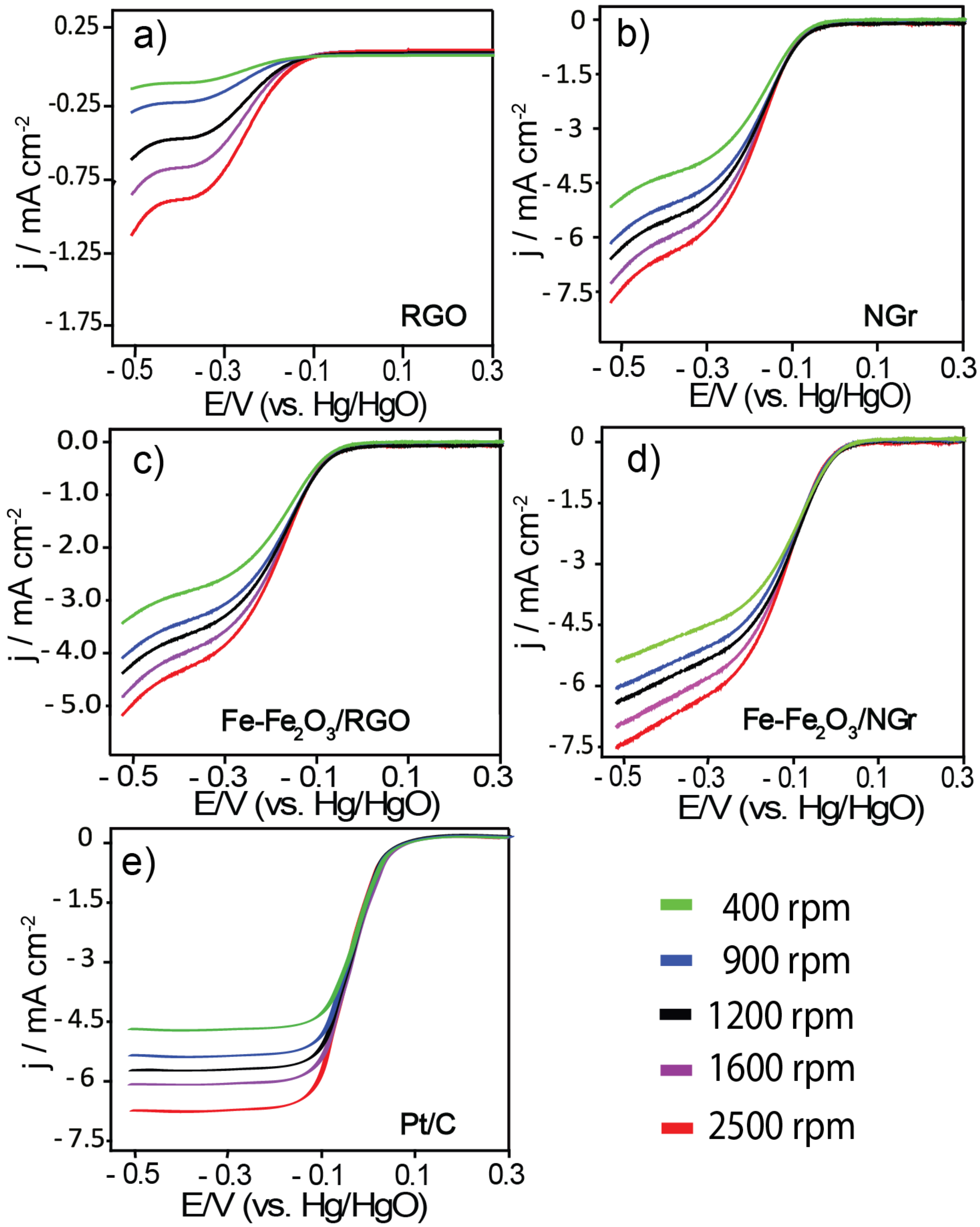

Figure S11: *Hydrodynamic study at different rotation rates of the working electrode in O_2-saturated alkaline electrolyte, (a) RGO, (b) NGr, (c) Fe-Fe_2O_3/RGO, (d) Fe-Fe_2O_3/NGr, and (e)Pt/C. Conditions: electrolyte: O_2-saturated 0.1 M KOH and scan rate: 10 mV/s.*

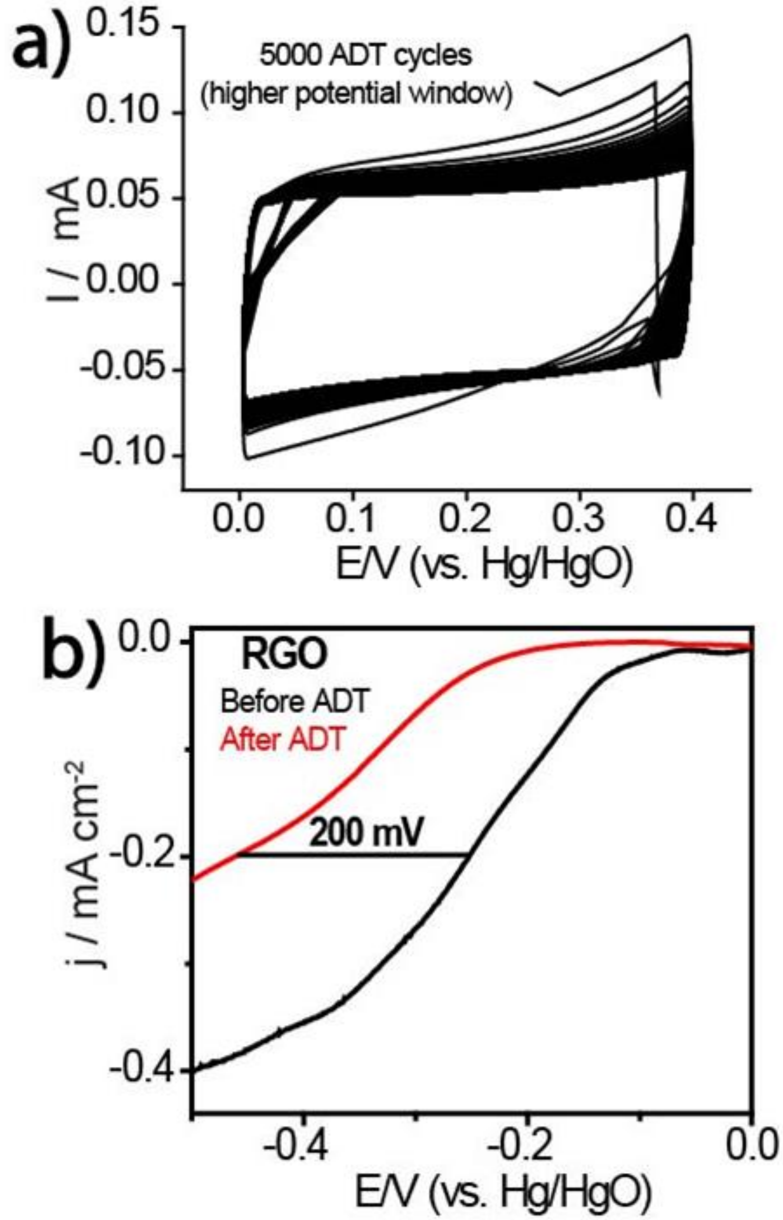

***Figure S12**: Accelerated durability test (ADT) of RGO in 0.1 M KOH. (a) 5000 potential cycles recorded at a scan rate of 50 mV/s in the potential window of 0.0 to 0.40 V (vs. Hg/HgO), and (b) comparative LSV curves before and after ADT, recorded at 10 mV/s.*

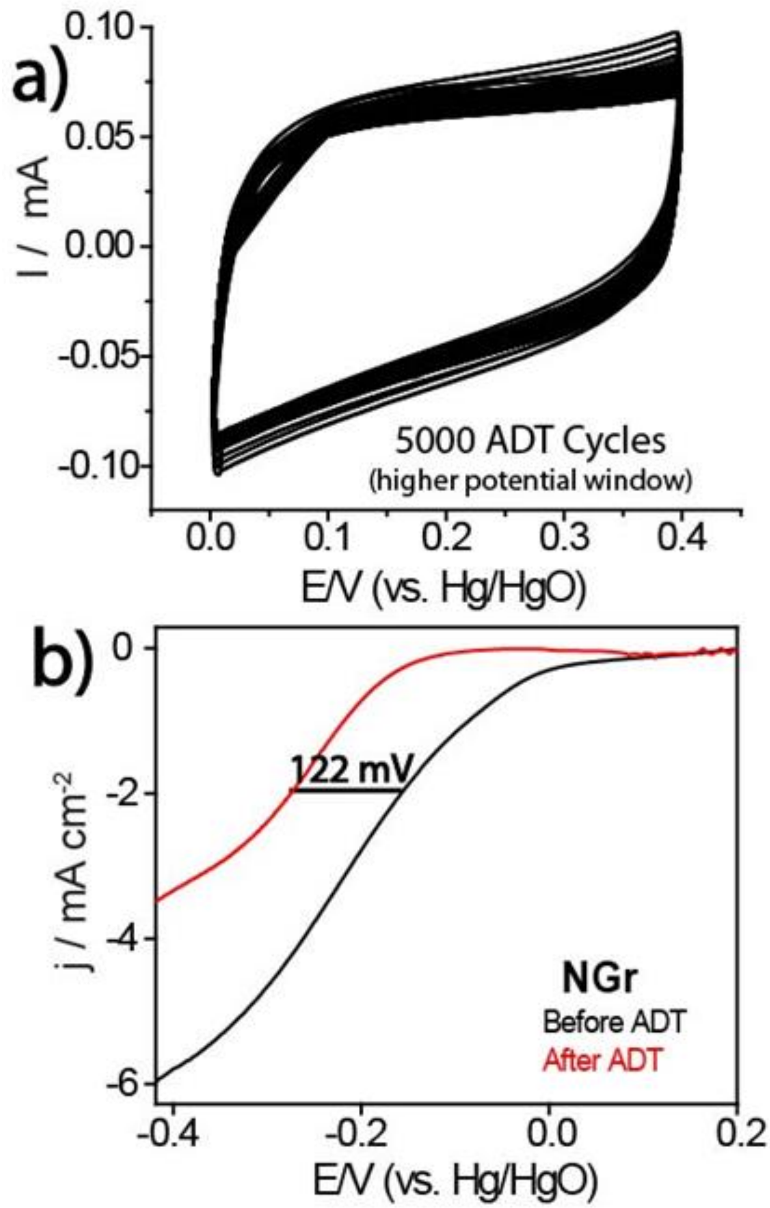

***Figure S13**: Accelerated durability test (ADT) of NGr in a 0.1 M KOH. (a) 5000 potential cycles recorded at a scan rate of 50 mV/s in the potential window of 0.0 to 0.40 V (vs. Hg/HgO), and (b) comparative LSV curves before and after ADT, recorded at 10 mV/s.*

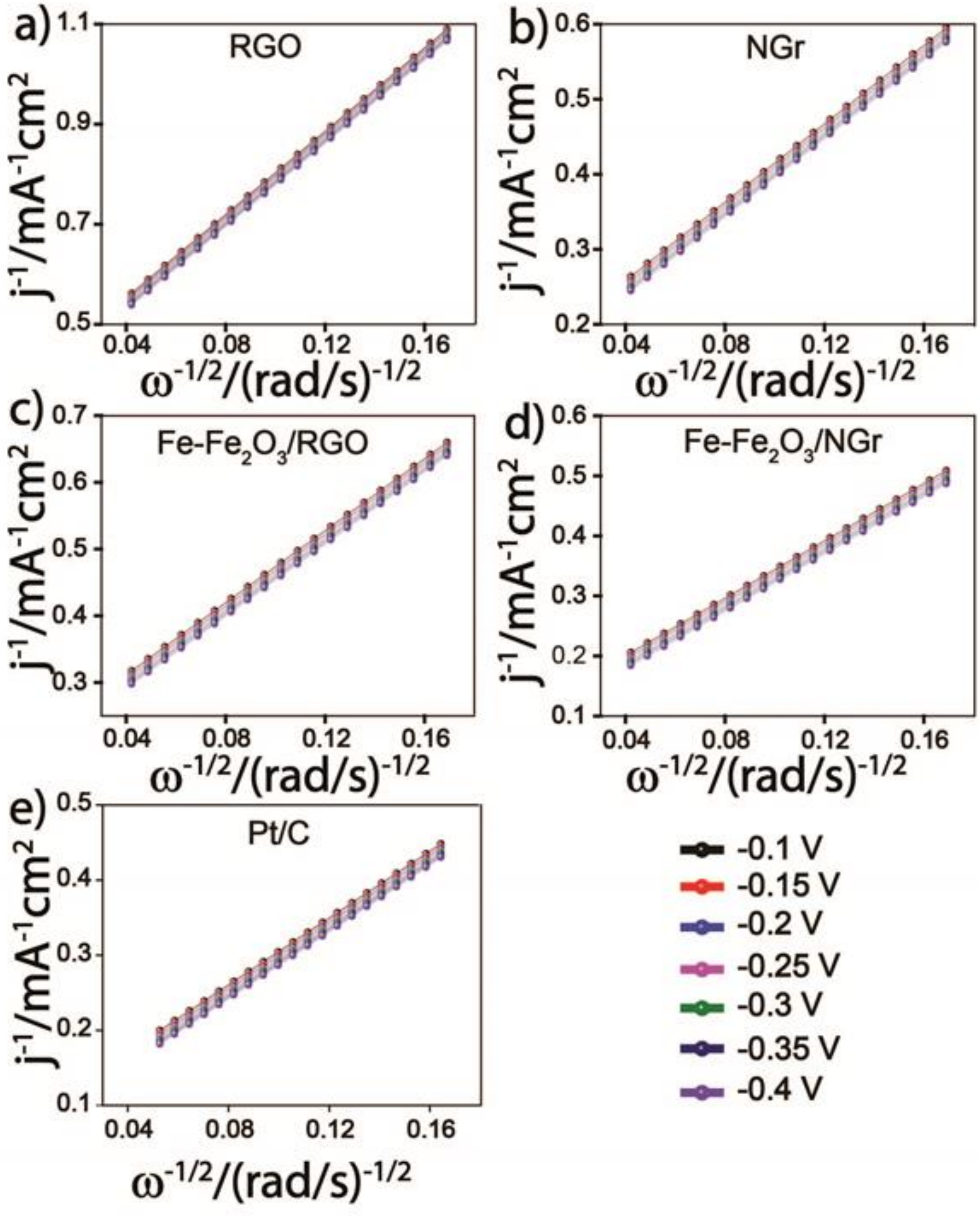

***Figure S14**: Koutecky-Levich (K-L) plots recorded at different potentials of (a) RGO, (b) NGr, (c) Fe-Fe_2O_3/RGO, (d) Fe-Fe_2O_3/NGr and (e) Pt/C.*

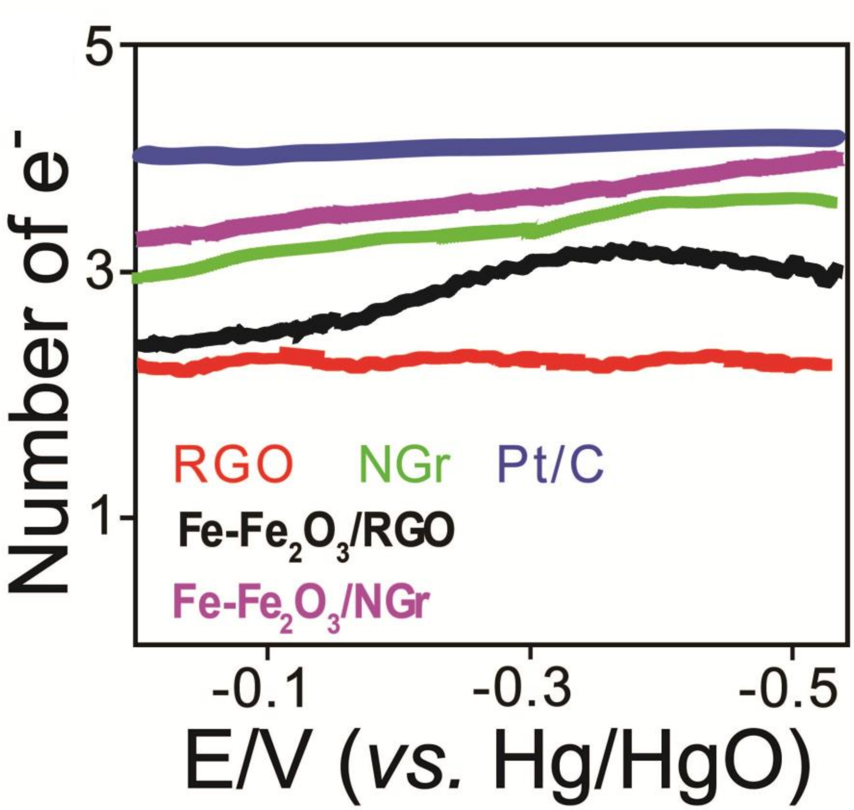

Figure S15: *Plots representing the calculated values of the number of electrons transferred with respect to the potential of the disc electrode.*

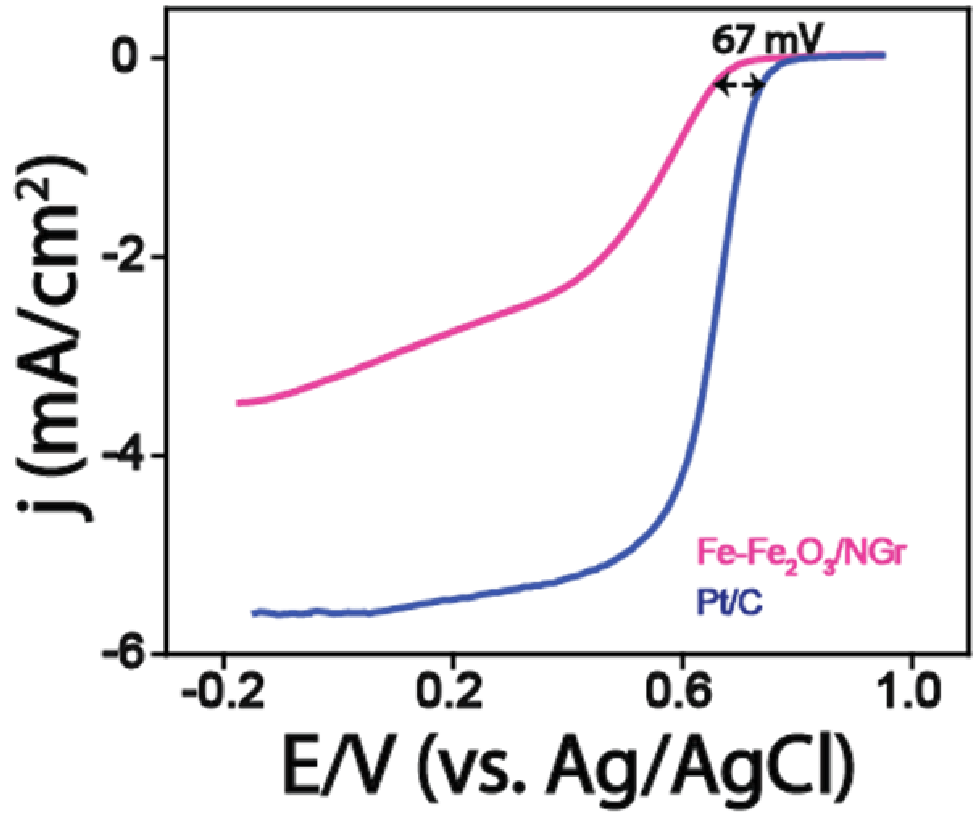

Figure S16: *Comparative LSVs of Fe-Fe_2O_3/NGr and Pt/C recorded at 1600 rpm. Conditions: electrolyte: O_2-saturated 0.1 M $HClO_4$ and scan rate: 10 mV/s.*

The obtained activity of Fe-Fe_2O_3/NGr in acidic condition is found to be less in comparison to the commercially available Pt/C. The onset potential of Fe-Fe_2O_3/NGr is found to ~ 67 mV shifted to the negative direction compared to Pt/C. Along with this, the limiting current is found to be ~5.8 and ~3.7 mA/cm^2 for Pt/C and Fe-Fe_2O_3/NGr, respectively. Overall, the lower activity of Fe-Fe_2O_3/NGr is mainly expected to be due to the direct exposure of the Fe-particles to the electrolyte and their subsequent leaching out issues under acid condition during the measurement. A comparison of the present data with the literature reported systems are presented in **Table S1**.

Table S1: *Comparison of the electrochemical data of systems reported in the literature with our system.*

Electrolyte	Electrocatalyst	Total Nitrogen Content	% of Pyridinic-N	% of Pyrrolic-N	% of Graphitic-N	ORR onset potential (V)	Limiting current density (mA/cm^2)	Reference
Acid	CNG-3	--	36.70 wt. %	18.60 wt. %	34.40 wt. %	~0.8 V (vs. RHE)	~4.0	1
Base	NGE-1000	7 wt. %	21 wt. %	53 wt. %	26 wt. %	~0.05 V (vs. Hg/HgO)	~4.5	2
Acid	Fe-PANI/C-Mela	--	24.2 wt. %	--	41.9 wt. %	0.98 V (vs. RHE)	~6.0	3
Acid	Fe-N-C-900	6.6 at %	61.4 %	27.9 %	10.7 %	0.8 V (vs. RHE)	~2.2	4
Base	Co-N-CNF	--	28.85	26.99	40.54	~-0.05 V (vs. Hg/HgO)	~3.5	5
Base	N-CNF	--	27.46	27.30	39.27	~0.05 V (vs. Hg/HgO)	~3.5	5
Base	Fe-N-C	3.08 at. %	1.1 %	1.82 %	0.16 %	1.05 V (vs. RHE)	~6.4	6
Base	Co-N-C	1.31 at.%	0.32 %	0.81 %	0.18 %	~0.95 V(vs. RHE)	~6.0	6
Base	NCNTa	2.35 at.%	14.83 at.%	68.20 at.%	16.96 at.%	-0.15 V (vs. Ag/AgCl)	3.19	7

Comparison of Electrochemical activity of different carbon morphologies reported in literature.

Electrolyte	Electrocatalyst	ORR onset potential (V)	Limiting current density (mA/cm^2)	Reference
Base	N-G-CNT	1.08 V (Vs. RHE)	~6.0	8
	N-CNT	~0.9 V (Vs. RHE)	~5.5	
Acid	N-G-CNT	~0.8 V (Vs. RHE)	~6.0	
	N-CNT	~0.7 V (vs. RHE)	~4.5	

Acid	PANI-Fe/Silica Colloid PANi-Fe/C (C: Vulcan XC-72)	~0.84 V (Vs. RHE) ~0.78 V (Vs. RHE)	4.4 3.3	9
Acid	FeCo/KB	~0.7 V (Vs. RHE)	~5.0	10
Acid	PANI/Fe/Vulcan XC PANI/Fe/KJ-300J PANI/Fe/BP-2000 PANI/Fe/MWCNTs	~0.89 V (Vs. RHE) 0.91 V (Vs. RHE) 0.91 V (Vs. RHE) 0.91 V (Vs. RHE)	~3.8 ~4.2 ~4.5 ~4.0	11
Base	Fe_3O_4/N-GAs	-0.19 V (vs. Ag/AgCl)	--	12
Acid	Fe_2O_3/Vulcan XC (No Nitrogen)	Very Poor Activity	~0.1	4
Base	NCNTa	-0.15 V (vs. Ag/AgCl)	3.19	7

Electrochemical activity of our electrocatalyst i.e. Fe-Fe_2O_3/NGr.

Electrolyte	**Electrocatalyst**	**Total Nitrogen Content**	**% of Pyridinic-N**	**% of Pyrrolic-N**	**% of Graphitic-N/ Quaternary-N**	**ORR onset potential (V)**	**Limiting current density (mA/cm^2)**	**Reference**
Base	Fe-Fe_2O_3/NGr	3.62 wt.%	42.50 wt.%	33.35 wt.%	18.75 wt. %	0.075 V (vs. Hg/HgO)	~7.0	**Present Work**
Acid	Fe-Fe_2O_3/NGr	3.62 wt. %	42.50 wt. %	33.35 wt. %	18.75 wt. %	0.633 V (vs. Ag/AgCl)	~3.7	**Present Work**

Table S2*: Single cell performance data and comparison with literature reports.*

Cathode Electrocatalyst	Cell temperature (°C)	Max. Power Density (mW/cm^2)	Reference
Fe/N/C	60	75	6
Co/N/C	60	68	6
NpGr-72	27	50	13
N-CNT	50	37	14
MnO/GC	70	98	15
Ag/C	25	10	16
CoPc/MWCNTs	50	120	17
FePc/MWCNTs	50	60	17
Au/C	50	36	18
Ag/C	50	19	18
FeN/ CNH-900	50	35	19
Fe-Fe_2O_3/NGr	60	54.40	**Present work**

References:

1. S. M. Unni, R. Illathvalappil, P. K. Gangadharan, S. N. Bhange, S. Kurugot, *Chem Commun.*, 2014, **50**, 13769.

2. S. M. Unni, S. Devulapally, N. Karjule, S. Kurungot, *J. Mater. Chem. A*, 2012, **22**, 23506

3. H. Peng, Z. Mo, S. Liao, H. Liang, L. Yang, F. Luo, H. Song, Y. Zhong, B. Zhang, *Sci. Rep.*, 2013, DOI: 10.1038/Srep01765.

4. C. H. Choi, S. Y. Lee, S. Park, S. I. Woo, *Appl. Cat. B: Environmental* 2011, **103**, 362.

5. D. Shin, B. Jeong, B. S. Mun, H. Jeon, H. J. Shin, J. Baik, J. Lee, *J. Phys. Chem. C* 2013, **117**, 11619.

6. J. Sanetuntikul, S. Shanmugam, *Nanoscale*, 2015, **7**, 7644.

7. Z. Chen, D. Higgins, Z. Chen, *Carbon*, 2010, **48**, 3057.

8. J. Shui, M. Wang, F. Du, L. Dai, *Sci. Adv.*, 2015. DOI: 10.1126/sciadv.1400129.

9. H. W. Liang, W. Wei, Z. S. Wu, X. Feng, K. Mullen, *J. Am. Chem. Soc.*, 2013, **135**, 16002.

10. J. Y. Cheon, T. Kim, Y. H. Choi, H. Y. Jeong, M. G. Kim, Y. J. Sa, J. Kim, Z. Lee, T. H. Yang, K. Kwon, O. Terasaki, G. G. Park, R. R. Adzic, S. H. Joo, *Sci. Rep.*, 2013, **3**, 2715.

11. G. Wu, K. L. More, P. Xu, H. L. Wang, M. Ferrandon, A. J. Kropf, D. J. Myers, S. Ma, C. M. Johnston, P. Zelenay, *Chem Commun.*, 2013, **49**, 3291.

12. Z. S. Wu, S. Yang, Y. Sun, K. Parvez, X. Feng, K. Mullen, *J. Am. Chem. Soc.*, 2012, **134**, 9082.

13. T. Palanisevam, M. O. Valappil, R. Illathvalappil, S. Kurungot, *Energy Environ. Sci.*, 2014, **7**, 1059.

14. C. V. Rao, Y. Ishikawa, *J. Phys. Chem. C*, 2012, **116**, 4340.

15. J. W. D. Ng, Y. Gorlin, D. Nordlund, T. F. Jaramillo, *J. Electrochem, Soc.*, 2014, **161**, D3105.

16. S. M. Maheshwari, P. Sridhar, S. Pitchumani, *Electrocatalysis*, 2011, **3**, 13-21.

17. I. Kruusenberg, L. Matisen, Q. Shah, A. M. Kannan, K. Tammeveski, *Int. J. Hydrogen Energy*, 2012, **37**, 4406.

18. S. D. Poynton, J. P. Kizewski, R. C. T. Slade, J. R. Varcoe, *Solid State Ionics*, 2010, **181**, 219.

19. S. M. Unni, S. Ramadas, R. Illathvalappil, S. N. Bhange, S. Kurungot, *J. Mater. Chem. A*, 2015, **3**, 4361.